Control of Semiconducting and Metallic Indium Oxide Nanowires

Taekyung Lim,[†] Sumi Lee,[†] M. Meyyappan,[‡,§] and Sanghyun Ju[†,*]

[†]Department of Physics, Kyonggi University, Suwon, Gyeonggi-Do, 443-760, Republic of Korea, [‡]NASA Ames Research Center, Moffett Field, California 94035, United States, and [§]IT Convergence Eng., POSTECH, Pohang, Republic of Korea

ABSTRACT Oxide semiconductors are candidates for chemical sensors, transparent electrodes, and electronic devices. Here, we have investigated metal-to-semiconductor transitions during In_2O_3 nanowire growth with variations in the O_2 gas rate. Photoluminescence and current–voltage characteristics of In_2O_3 nanowire transistors have been used to understand the transition behavior. The proportion of metallic nanowires to semiconducting nanowires significantly changes from 80:20 to 25:75 when the O_2 fraction in argon increases from 0.005% to 0.2%. We believe that excessive oxygen vacancies at low O_2 gas rates increase the conductivity and thereby the number of nanowires with metallic characteristics. With an increase in oxygen flow, the oxygen vacancies in the nanowires are substituted with oxygen and the subsequent reduction in oxygen vacancies increases the number of semiconducting nanowires. The threshold voltage of transistors fabricated with semiconducting nanowires shifts in a positive direction by about +3.3 eV between nanowires grown with 0.005% and 0.2% oxygen. The results here indicate that electrical and optical characteristics of oxide nanowires can be controlled by the amount of oxygen during growth instead of relying on conventional postgrowth high-temperature annealing or other postprocessing techniques.

KEYWORDS: semiconductor · metal · oxygen vacancy · oxide nanowire · In_2O_3 · threshold voltage

Miniaturization of electronic, optoelectronic, and sensing devices has recently entered into the nanoscale era.[1−4] In this regard, one-dimensional nanowires of various inorganic materials have received much attention in recent years.[5] Oxide nanowires such as ZnO, SnO_2, and In_2O_3 have been considered to be candidates for transistors, chemical and biosensors, and transparent conducting electrodes.[5−12] Consistency and improvement in performance in all these applications requires control of the nanowire surface quality and properties, and this has been done by plasma or ozone treatment of synthesized nanowires and the use of organic insulators.[13−15] In addition, conventional high-temperature annealing has also been shown to improve the crystalline quality of oxide nanowires and reduce oxygen vacancies.[16,17] In contrast to such postprocessing modifications, it is desirable to optimize growth conditions and control the nanowire properties during growth.[18] Here, we demonstrate such an approach in the growth of In_2O_3 nanowires and report the transition of nanowire properties from metal to semiconductor by appropriately controlling the O_2 rate in the input gas stream.

RESULTS AND DISCUSSION

In_2O_3 nanowires were grown by chemical vapor deposition (CVD) on SiO_2/Si wafer substrates coated with 20 nm sized gold particles as the catalyst. The InAs target was placed 16 cm from the substrate in a horizontal quartz tube chamber. The temperature of the InAs target was increased to 800 °C, while that of the substrate zone was set to 750 °C. The two gases—Ar and Ar:O_2 (6%)—were mixed at five different rates (Ar with 0.005%, 0.01%, 0.06%, 0.1%, and 0.2% O_2), and the total flow rate was maintained at 96 sccm. The reaction time was 120 min in all cases.

The nanowires were first characterized through field emission scanning electron microscopy (FE-SEM) and X-ray energy-dispersive spectroscopy (EDS). As shown in Figure 1a, nanowires of average diameter (d) = 60 nm and L = ∼10 μm steadily grew regardless of the O_2 gas rate. However, the density of the nanowires appears to be influenced by the oxygen ratio. In addition, when the O_2 ratio in argon exceeded 0.2%, the growth rate sharply decreased and the nanowires did not grow properly; instead, only nanoparticles or thin films were observed. The EDS analysis of the surface of the nanowires in the five cases is shown in the insets of each image, which confirms the presence of indium (In) and oxygen (O). X-ray diffraction (XRD) analysis was performed to verify the nanowire crystal structures as shown in Figure 1b. Three major diffraction peaks can be seen in (222), (400), and (441), which are equivalent to the line spectrum of bulk In_2O_3 having a cubic structure of lattice constant a = 1.012 nm (ICDD File No. 76-0152); thus, the synthesized nanowires are definitely In_2O_3. However, the crystal structures here do not seem

* Address correspondence to shju@kgu.ac.kr.

Received for review January 31, 2011 and accepted April 19, 2011.

Published online April 19, 2011
10.1021/nn200390d

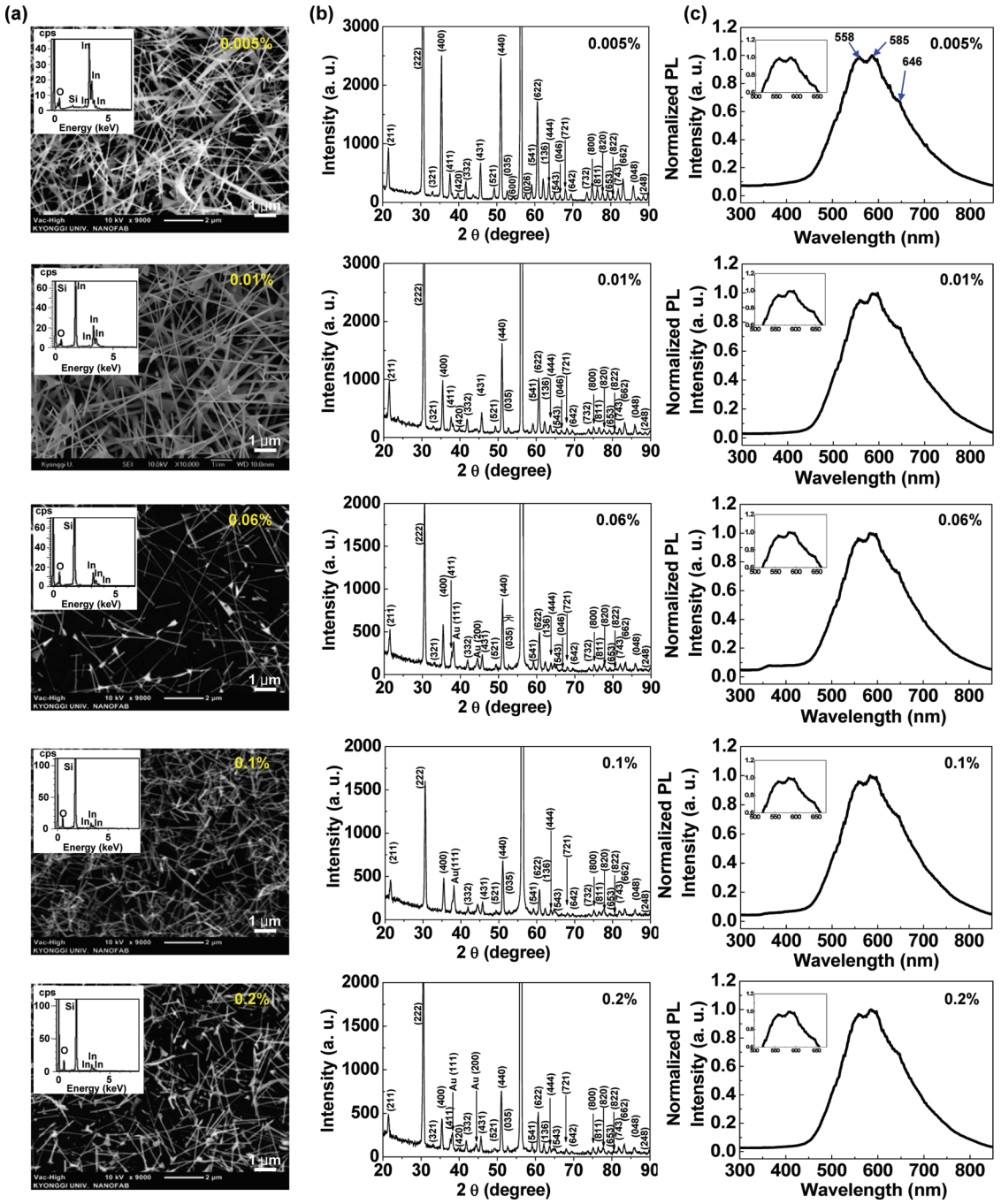

Figure 1. In_2O_3 nanowires grown at five different oxygen flow rates (Ar with 0.005%, 0.01%, 0.06%, 0.1%, and 0.2% O_2): (a) FE-SEM images. (b) XRD spectra. (c) Room-temperature PL spectra.

to vary with the amount of O_2 used for growth. Note that the strong peak of around 56°, between the (440) and (622) peaks, is the silicon (311) peak corresponding to the silicon substrate.

Oxygen vacancies are generally known to be common defects in poly- and nanocrystalline oxides and act as radiative centers and also as radiative traps in luminescence processes. They can form defect levels in the gap and contribute to the midgap luminescence. Figure 1c shows the photoluminescence (PL) spectra for each of the cases studied here. The origins of the PL spectrum in In_2O_3 are not clear according to previous reports on indium oxide thin films, particles, and nanowires, but they have been assumed to be due to oxygen vacancies or deficiencies produced during the growth process.[19−23] Also, oxygen vacancies lead to new energy levels within the bandgap in various ways, and they cause different emissions peaks to be exhibited.[19,20] For oxygen deficiencies, peaks at 430, 480, 520, 470, and 637 nm have been seen, whereas peaks at 570, 580, and 630 nm have been reported for oxygen vacancies in In_2O_3.[20,23] The 630 nm peak is also

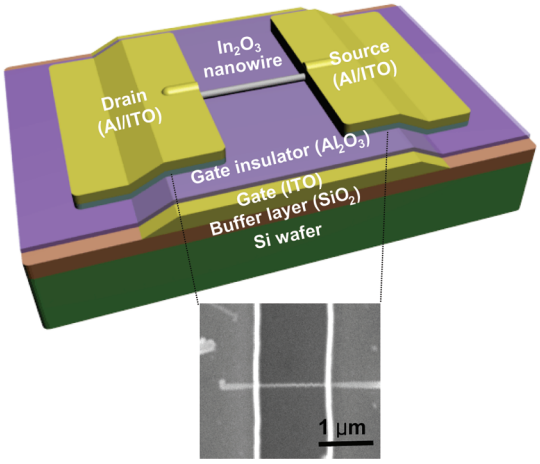

Figure 2. Schematic of the bottom-gated In_2O_3 nanowire transistor and an SEM image of the device.

attributed to intrinsic defects related to oxygen rather than oxygen vacancies in In_2O_3 nanowires.[24] As shown in Figure 1c, green emission, yellow emission, and weak shoulder peaks can be observed at 558, 585, and 646 nm, respectively. The locations of the peaks do not seem to change with the amount of oxygen in the feedstock; however, the ratio of the 558 nm peak intensity to 585 nm peak intensity (I_{558}/I_{585}) and 646 nm peak intensity appears to vary. When the O_2 fraction is 0.005%, I_{558}/I_{585} is around ~1; however, when the fraction exceeds 0.01%, this ratio is around 0.97. These PL emission peaks (558 and 585 nm) are based on the combination between photogenerated holes and electrons in oxygen vacancies (for instance, whether two-electron captured state, singly ionized state, or doubly ionized state). On the basis of the decreased peak intensity, it is probable that the oxygen vacancy related to 558 nm (2.2 eV) decreases by O_2 injection. Moreover, the shoulder of the 646 nm peak slightly increases when the O_2 gas rate increases from 0.005% to more than 0.1%. We believe that the intrinsic defects related to oxygen, such as interstitial oxygen, indium vacancy, and antisite oxygen, slightly increase with the O_2 gas injection. The electrical characteristics of metal oxide nanowires are largely influenced by the oxygen vacancy; particularly, their conductance is determined by singly or doubly ionized surface oxygen vacancy.[25] Therefore, nanowire transistors (NWTs) were fabricated using nanowires synthesized with various O_2 flow rates in order to examine the change in electrical characteristics of the devices. In addition, the changes in transistor characteristics and their relationship with the amount of oxygen vacancy were analyzed.

Figure 2 shows a cross-sectional view of the bottom-gated In_2O_3 NWT, and the inset is an FE-SEM image of the nanowire channel region. In this study, 20−30 In_2O_3 NWTs were fabricated for each O_2 gas rate and analyzed in a statistical manner. In all cases, nanowires close to 60 nm in diameter were chosen to isolate the impact of the oxygen flow rate. It is noteworthy that the investigated NWTs for each O_2 rate case have a distribution of devices with some showing ideal semiconducting characteristics and the remaining with ideal metallic characteristics. In the case of nanowires grown with low oxygen ratios (LOR), most of the devices exhibit metallic behavior. However, the fraction of devices with semiconducting behavior increases with an increase in the oxygen ratio during growth; in addition, a positive shift in threshold voltage (V_{th}) is seen in these semiconducting NWTs.

Figure 3a shows the drain current *versus* gate −source voltage ($I_{ds}-V_{gs}$) characteristics of eight representative metallic devices from each oxygen pressure. An almost constant current of around 5−100 μA flows at V_{ds} of 0.5 V irrespective of the gate voltages. Moreover, in the case of the drain current *versus* drain−source voltage ($I_{ds}-V_{ds}$) curve shown in the inset of Figure 3a, the current does not saturate but continues to increase linearly with the drain voltage. In addition, the current also increases with gate voltage, though the effect is very small. In other words, the In_2O_3 nanowires do not exhibit semiconductor characteristics when the current flows in the channel under the influence of the gate voltage, instead they exhibit metallic characteristics as the source and drain are connected to metal lines.

The influence of the O_2 gas rates on the electrical characteristics of In_2O_3 NWTs that exhibit semiconductor characteristics was also examined. Figure 3b shows the $I_{ds}-V_{gs}$ curve of those NWTs for each O_2 gas rate. Although nanowires grown with different O_2 gas rates lead to different transistor characteristics, V_{th} is generally around −9 V at 0.005%; this represents a larger negative shift than in previous reports, for example, −2.0 to −3.5 V for SnO_2 and ZnO devices and −5 V for In_2O_3 vertical transistors.[11,12,26,27] The significantly large V_{th} here is considered to be a result of numerous oxygen vacancies on the surface of the nanowires. The inset in Figure 3b indicates linear $I_{ds}-V_{gs}$ curves for each O_2 flow rate. The V_{th} exhibits a positive shift with the flow rate increase, changing from −9 V at 0.005% to −5.7 V at 0.2%. The oxygen vacancy decreases as O_2 substitutes for the large number of vacancies existing in the In_2O_3 nanowire. Consequently, V_{th} of n-type In_2O_3 NWTs exhibits a positive shift due to the decrease, since the oxygen vacancy plays the role of a donor in nanowires. However, the V_{th} positive shift is not in a linear relationship with the flow rate; for instance, when the flow rate is over 0.1%, V_{th} hardly exhibits any shift. Thus, the change in electrical characteristics with oxygen vacancy seems to saturate beyond a certain flow rate. Besides V_{th}, the on-current (I_{on}) varies in the range 1−1.7 μA depending on the O_2 rates; the on−off current ratio (I_{on}/I_{off}) is ~10^5, and the effective mobility (μ_{eff}) is 41−57 $cm^2/V\cdot s$. The subthreshold ratio (SS) increases from 0.1 V/decade at

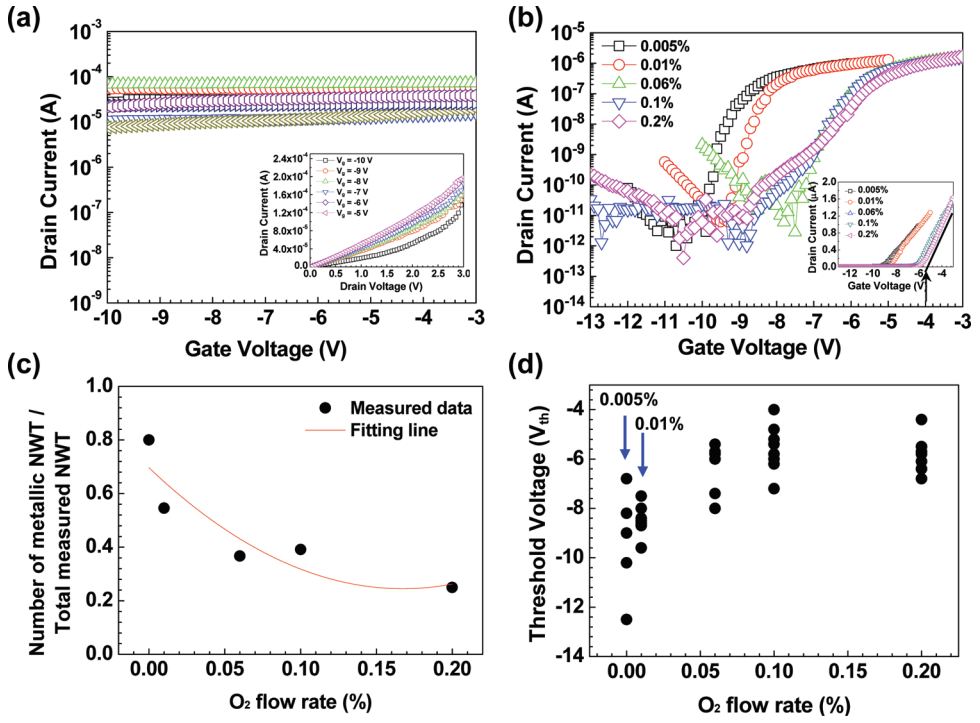

Figure 3. In_2O_3 NWT characteristics: (a) Drain current *versus* gate−source voltage (I_{ds}−V_{gs}) of the metallic In_2O_3 devices randomly selected from different O_2. The inset displays the corresponding drain current *versus* drain−source voltage (I_{ds}−V_{ds}) characteristics. V_{ds} = 0.5 V. (b) Log-scale drain current *versus* gate−source voltage (I_{ds}−V_{gs}) of the semiconducting In_2O_3 NWTs. The inset is the linear-scale drain current *versus* gate−source voltage (I_{ds}−V_{gs}) characteristics of In_2O_3 NWTs. V_{ds} = 0.5 V. (c) Ratio of the metallic NWTs to the total number of measured devices plotted against the O_2 flow rate used in growth. The total measured devices consist of metallic and semiconducting NWTs. (d) The impact of oxygen flow rate on the variation of V_{th}.

0.005% to 0.20 V/decade at 0.06% and 1.2 V/decade at 0.2%, thereby indicating an increasing trend of the slope with increasing O_2 gas rates. We believe that the SS increases due to the increase in the 646 nm peak shown in the PL spectrum, or, in other words, the increase in the oxygen-related intrinsic defects.

The influence of different O_2 gas rates on the frequency of finding nanowires with metallic or semiconductor characteristics is shown in Figure 3c. The ratio of nanowires with metal characteristics to semiconductor characteristics is 80:20, 55:45, 37:63, 39:61, and 25:75 at O_2 gas rates of 0.005%, 0.01%, 0.06%, 0.1%, and 0.2%, respectively; this indicates that the number of devices with metallic characteristics decreases, while those with semiconducting characteristics increase when the oxygen feed ratio increases in the growth reactor. The excessive oxygen vacancies mentioned earlier increase the conductivity, leading to more devices with metallic characteristics; however, the oxygen vacancies are substituted with an increasing amount of oxygen in the feedstock, which consequently decreases the number of devices with metallic characteristics, as shown in Figure 3c. Statistical variations in V_{th} are captured in Figure 3d, which shows a shift in the positive direction with an increase in O_2 rate in the input, as mentioned earlier. The transistor characteristics show a saturation behavior at high oxygen ratios above 0.1% (not shown here), and as a result, V_{th} remains constant after some critical oxygen ratio. Oxygen vacancies play the role of donors, and their reduction creates a positive shift in V_{th} in n-type In_2O_3 NWTs.

In summary, we have shown a shift in the quantity of In_2O_3 nanowires with metallic characteristics to the semiconducting variety when the amount of oxygen in the input gas stream is varied during the CVD process. The transition is the result of changes in oxygen vacancies and deficiencies in the nanowires, which are influenced by the oxygen rate. Data from PL and electrical measurements support this observation. Until now, electrical and optical properties of as-grown nanowires have been manipulated only by postgrowth annealing. For example, orange luminescence at 590 nm in SnO_2 nanowires has been shown to decrease after a 2 h annealing in oxygen because oxygen vacancies are supplied with oxygen.[16,17] The *in situ* control during growth offered by changing the gas flow composition is a preferable one-step alternative to postprocessing techniques, thus saving significant time and thermal budget. The results from this study have implications in sensor and other electronics applications, as vacancy concentrations and chemical structures affect electrical and optical properties. Considering chemical sensors as an example, nanowire transistors or chemiresistors exhibit a change in conductance when exposed to an analyte.[8,9] The sensors generally have oxygen-derived adsorbates on the

nanowire surface that deplete the electrons near the surface, resulting in a lower conductance state. When this surface layer is exposed to a reducing gas during sensor operation, the conductance increases with a release of electrons back to the conductance band following surface reactions. The ability to tailor nanowire properties demonstrated here is expected to be useful in such applications.

METHODS

Fabrication and Analysis of In_2O_3 NWTs. The bottom-gated In_2O_3 nanowire transistors were fabricated in the following manner. First, indium tin oxide (ITO) (~100 nm thickness) was patterned on thermally grown SiO_2/Si wafers used as gate electrodes. Al_2O_3 (~30 nm thickness with a dielectric constant $\varepsilon \sim 9$) was deposited as a gate insulator using atomic layer deposition. The gate contact pad area was then opened by contact etching. Subsequently, the In_2O_3 nanowire was dispersed on top of the Al_2O_3-deposied gate electrode region to create the channel. Finally, an Al/ITO metal bilayer was deposited and patterned at both ends of the nanowire to create the source and drain electrodes. The electrical characteristics of the transistors were measured by a semiconductor parameter analyzer (Agilent B1500A). The performance of all the NWTs was compared using the threshold voltage (V_{th}) obtained by the transconductance method, the on-current (I_{on}: I_{ds} at $V_{gs} = V_{th} + 3$ V and $V_{ds} = 0.5$ V), on−off current ratio (I_{on}/I_{off}), subthreshold ratio (SS), and effective mobility (μ_{eff}). μ_{eff} was calculated using $\mu_{eff} = dI_{ds}/dV_{gs} \times L^2/C_i \times 1/V_{ds}$ where C, the gate-to-channel capacitance, is given by $C_i = 2\pi\varepsilon_0 k_{eff} L/\cosh^{-1}(1 + t_{ox}/r)$. The effective dielectric constant of Al_2O_3 (k_{eff}) is ~9.0; the device channel length (L) is 1.5−3.0 μm; and the radius (r) of the In_2O_3 nanowire is ~30 nm.

Acknowledgment. This research was supported by the Converging Research Center Program through the National Research Foundation of Korea (NRF) funded by the Ministry of Education, Science and Technology (2010K000990 and 2010-0019108). Acknowledgement is also due to WCU Program at POSTECH through the National Research Foundation of Korea funded by the Ministry of Education, Science and Technology (R31-2008-000-10100-0).

REFERENCES AND NOTES

1. Cui, Y.; Lieber, C. M. Functional Nanoscale Electronic Devices Assembled Using Silicon Nanowire Building Blocks. *Science* **2001**, *291*, 851–853.
2. DeHon, A. Array-Based Architecture for FET-Based, Nanoscale Electronic. *IEEE Trans. Nanotechnol.* **2003**, *2*, 23–32.
3. Zhong, Z.; Qian, F.; Wang, D.; Lieber, C. M. Synthesis of P-Type Gallium Nitride Nanowires for Electronic and Photonic Nanodevices. *Nano Lett.* **2003**, *3*, 343–346.
4. Mcalpine, M. C.; Ahmad, H.; Wang, D.; Heath, J. R. Highly Ordered Nanowire Arrays on Plastic Substrates for Ultrasensitive Flexible Chemical Sensors. *Nat. Mater.* **2007**, *6*, 379–384.
5. Meyyappan, M.; Sukara, M. K. *Inorganic Nanowires: Applications, Properties and Characterization*; CRC Press: Boca Raton, FL, 2010.
6. Ju, S.; Facchetti, A.; Xuan, Y.; Liu, J.; Ishikawa, F.; Ye, P.; Zhou, C.; Marks, T. J.; Janes, D. B. Fabrication of Fully Transparent Nanowire Transistors for Transparent and Flexible Electronics. *Nat. Nanotechnol.* **2007**, *2*, 378–384.
7. Zhang, W. F.; He, Z. B.; Yuan, G. D.; Jie, J. S.; Luo, L. B.; Zhang, X. J.; Chen, Z. H.; Lee, C. S.; Zhang, W. J.; Lee, S. T. High-Performance, Fully Transparent, and Flexible Zinc-Doped Indium Oxide Nanowire Transistors. *Appl. Phys. Lett.* **2009**, *94*, 123103.
8. Xiangfeng, C.; Caihong, W.; Dongli, J.; Chenmou, Z. Ethanol Sensor Based on Indium Oxide Nanowires Prepared by Carbothermal Reduction Reaction. *Chem. Phys. Lett.* **2004**, *399*, 461–464.
9. Zhang, D.; Li, C.; Liu, X.; Han, S.; Tag, T.; Zhou, C. Doping Dependent NH_3 Sensing of Indium Oxide Nanowires. *Appl. Phys. Lett.* **2003**, *83*, 1845–1847.
10. Curreli, M.; Li, C.; Sun, Y.; Lei, B.; Gunderson, M. A.; Thompson, M. E.; Zhou, C. Selective Functionalization of In_2O_3 Nanowire Mat Devices for Biosensing Applications. *J. Am. Chem. Soc.* **2005**, *127*, 6922–6923.
11. Nguyen, P.; Ng, H. T.; Yamada, T.; Smith, M. K.; Li., J.; Han, J.; Meyyappan, M. Direct Integration of Metal Oxide Nanowire in Vertical Field-Effect Transistor. *Nano Lett.* **2004**, *4*, 651–657.
12. Ng, H. T.; Han, J.; Yamada, T.; Nguyen, P.; Chen, Y. P.; Meyyappan, M. Single Crystal Nanowire Vertical Surround-Gate Field-Effect Transistor. *Nano Lett.* **2004**, *4*, 1247–1252.
13. Ra, H. -W.; Khan, R.; Kim, J. T.; Kang, B. R.; Bai, K. H.; Im, Y. H. Effects of Surface Modification of the Individual ZnO Nanowire with Oxygen Plasma Treatment. *Mater. Lett.* **2009**, *63*, 2516–2519.
14. Ju, S.; Lee, K.; Yoon, M. -H.; Facchetti, A.; Marks, T. J.; Janes, D. B. High Performance ZnO Nanowire Field Effect Transistors with Organic Gate Nanodielectrics: Effects of Metal Contacts and Ozone Treatment. *Nanotechnology* **2007**, *18*, 155201.
15. Ju, S.; Lee, K.; Janes, D. B. Low Operating Voltage Single ZnO Nanowire Field-Effect Transistors Enabled by Self-Assembled Organic Gate Nanodielectrics. *Nano Lett.* **2005**, *5*, 2281–2286.
16. Kar, A.; Yang., J.; Dutta, M.; Stroscio, M. A.; Kumari, J.; Meyyappan, M. Rapid Thermal Annealing Effects on Tin Oxide Nanowires Prepared by Vapor−Liquid−Solid Technique. *Nanotechnology* **2009**, *20*, 065704.
17. Kar, A.; Stroscio, M. A.; Dutta, M.; Kumari, J.; Meyyappan, M. Growth and Properties of Tin Oxide Nanowires and the Effect of Annealing Conditions. *Semicond. Sci. Technol.* **2010**, *25*, 024012.
18. Hong, W. K.; Sohn, J. I.; Hwang, D. K.; Kwon, S. S.; Jo, G.; Song, S.; Kim, S. M.; Ko, H. J.; Park, S. J.; Welland, M. E.; Lee, T.; *et al.* Tunable Electronic Transport Characteristics of Surface-Architecture-Controlled ZnO Nanowire Field Effect Transistors. *Nano Lett.* **2008**, *8*, 950–956.
19. Liang, C.; Meng, G.; Lei, Y.; Phillipp, F.; Zhang, L. Catalytic Growth of Semiconducting In_2O_3 Nanofibers. *Adv. Mater.* **2001**, *13*, 1330–1333.
20. Jeong, J. S.; Lee, J. Y.; Lee, C. J.; An, S. J.; Yi, G.-C. Synthesis and Characterization of High-Quality In_2O_3 Nanobelts via Catalyst-Free Growth Using a Simple Physical Vapor Deposition at Low Temperature. *Chem. Phys. Lett.* **2004**, *384*, 246–250.
21. Zhou, H. J.; Cai, W. P.; Zhang, L. D. Photoluminescence of Indium−Oxide Nanoparticles Dispersed within Pores of Mesoporous Silica. *Appl. Phys. Lett.* **1999**, *75*, 495–497.
22. Lee, M. S.; Choi, W. C.; Kim, E. K.; Kim, C. K.; Min, S. K. Characterization of the Oxidized Indium Thin Films with Thermal Oxidation. *Thin Solid Films* **1996**, *279*, 1–3.
23. Jean, S. T.; Her, Y. C. Growth Mechanism and Photoluminescence Properties of In_2O_3 Nanotowers. *Cryst. Growth Des.* **2010**, *10*, 2104–2110.
24. Mazzera, M.; Zha, M.; Calestani, D.; Zappettini, A.; Lazzarini, L.; Salviati, G.; Zanotti, L. Low-Temperature In_2O_3 Nanowire Luminescence Properties as a Function of Oxidizing Thermal Treatments. *Nanotechnology* **2007**, *18*, 355707.

25. Kolmakov, A.; Moskovits, M. Chemical Sensing and Catalysis by One-Dimensional Metal-Oxide Nanostructures. *Annu. Rev. Mater. Res.* **2004**, *34*, 151.
26. Ju, S.; Chen, P.; Zhow, C.; Ha, Y.; Facchetti, A.; Marks, T. J.; Kim, S.; Mohammadi, S.; Janes., D. B. 1/f Noise of SnO_2 Nanowire Transistors. *Appl. Phys. Lett.* **2008**, *92*, 243120.
27. Ju, S.; Li, J.; Pimparkar, N.; Alam, M. A.; Chang, R. P. H.; Janes, D. B. N-Type Field-Effect Transistors using Multiple Mg-doped ZnO Nanorods. *IEEE Trans. Nanotechnol.* **2007**, *6*, 390–395.